Eur. Phys. J. A **22**, 363–370 (2004)
DOI 10.1140/epja/i2004-10054-4

THE EUROPEAN PHYSICAL JOURNAL A

The two-proton shell gap in Sn isotopes

P. Fleischer[1], P. Klüpfel[1], T. Cornelius[2], T.J. Bürvenich[3], S. Schramm[2], J.A. Maruhn[2], and P.-G. Reinhard[1,a]

[1] Institut für Theoretische Physik, Universität Erlangen, Staudtstrasse 7, D-91058 Erlangen, Germany
[2] Institut für Theoretische Physik, Universität Frankfurt, D-60325 Frankfurt, Germany
[3] Theoretical Division, Los Alamos National Laboratory, Los Alamos, NM 87545, USA

Received: 11 May 2004 / Revised version: 14 July 2004 /
Published online: 16 November 2004 –
Communicated by G. Orlandini

Abstract. We present an analysis of two-proton shell gaps in Sn isotopes. As theoretical tool we use self-consistent mean-field models, namely the relativistic mean-field model and the Skyrme-Hartree-Fock approach, both with two different pairing forces, a delta interaction (DI) model and a density-dependent delta interaction (DDDI). We investigate the influence of nuclear deformation as well as collective correlations and find that both effects contribute significantly. Moreover, we find a further significant dependence on the pairing force used. The inclusion of deformation plus correlation effects and the use of DDDI pairing provides agreement with the data.

PACS. 21.10.Dr Binding energies and masses – 21.10.Pc Single-particle levels and strength functions – 21.60.Jz Hartree-Fock and random-phase approximations – 24.10.Jv Relativistic models

1 Introduction

Understanding nuclear shell structure has been a key issue of nuclear physics for decades [1,2]. It remains a topic of large current interest in connection with nuclei far from the valley of stability for which a large pool of new data is now available [3]. The predictive value of nuclear structure models in the various regimes of exotic nuclei depends very much on their ability to describe shell structure in quantitative detail, particularly for superheavy nuclei with their subtle dependence on shells [4,5]. On the other hand, there is the basic problem that we do not dispose of observables which give direct experimental access to the single-particle levels of nuclei. There is the seemingly "direct" deduction through separation energies and excitation spectra of neighboring odd nuclei. The proper modeling of these observables by mean-field models, however, is rather involved as it requires inclusion of a proper blocking description, polarization effects and breaking of time-reversal symmetry [6,7]. It is desirable to have complementing information on the single-particle structure and one hopes that data deduced only from even-even nuclei give simpler access to spectral gaps. In this context the two-nucleon shell gaps are often considered [8]. They are simply the second differences of binding energies and thus easily available from experiment. The workload comes on the theoretical side because this quantity, being a difference of large numbers, is extremely sensitive to all sorts of corrections and thus requires careful modeling. Systematic measurements on the long chain of Pb isotopes [3,9] have shown a steady decrease of the two-proton shell gap towards the proton drip line indicating some shell quenching. It was found in a subsequent theoretical analysis that deformation masks the data such that the two-proton shell gap shows a quenching while the spectral gap does not [10]. Proper inclusion of deformed mean fields brought satisfactory agreement with the experimental results. It is the aim of the present paper to continue these investigations for a different test case, namely the two-proton shell gap in the chain of Sn isotopes. It will turn out that deformation effects are as important as they were in the case of the Pb isotopes, but we will find also that ground-state deformation alone is insufficient to explain the experimental two-proton shell gaps in Sn. Thus we have extended the studies to include a new aspect, namely the effect of collective ground-state correlations on the two-proton shell gaps. We will consider two brands of mean-field models, namely the relativistic mean-field model (RMF) as well as the non-relativistic Skyrme-Hartree-Fock (SHF) approach and a variety of parameterizations within both models. For technical reasons, the study of ground-state correlations is confined to SHF models.

The paper is outlined as follows: In sect. 2, we very briefly explain the formal framework, the mean-field models and the treatment of collective correlations. In sect. 3, we present and discuss the results, where subsect. 3.1 is concerned with deformed mean-field states and subsect. 3.2 with the impact of ground-state correlations.

[a] e-mail: reinhard@theorie2.physik.uni-erlangen.de

2 Framework

2.1 Self-consistent mean-field models

Our investigation is performed in the framework of self-consistent mean-field theories, namely the non-relativistic Skyrme-Hartree-Fock approach (SHF) and the relativistic mean-field (RMF) model, for the formal details and an extensive discussion of their properties see [11]. Moreover, we employ for the RMF two slightly different brands, namely the traditional variant with finite-range meson exchange (RMF-FR) [12,13] and the more recent version employing point couplings (RMF-PC) [14,15]. This span of models explores different physical ingredients: a comparison of SHF with RMF tests the non-relativistic *versus* relativistic approach, the comparison of RMF-FR and RMF-PC tests the importance of finite-range mean fields. In each of these models, there exists a great variety of different parameterizations which all deliver a comparable and excellent description of bulk properties in stable nuclei but can differ substantially in the realm of exotic nuclei or when looking at more subtle observables, as we will do here. One thus has to use in such investigations a representative sample of different parameterizations to disentangle genuine mean-field effects from particularities of a given parameterization. From the SHF family we will consider: SkM* as a widely used traditional standard [16], Sly6 as a recent fit which includes information on isotopic trends and neutron matter [17], SkI3 as a fit which maps the relativistic isovector structure of the spin-orbit force and takes care of the surface thickness [18], and SkO [19] as a recent fit in a similar fashion as SkI3 but with bias on a larger effective mass and a better adjusted asymmetry energy. For the RMF model, we consider the RMF-FR parameterizations NL-Z2 [20] and NL3 [21] as well as the RMF-PC force PC-F1 [15]. Both NL-Z2 and PC-F1 have been fitted to a similar set of data as SkI3 and SKO, including information on the nuclear charge form factor. NL3 has been adjusted with particular emphasis on isovector properties and incompressibility. For all models, pairing is added at the level of BCS with Lipkin-Nogami correction. We use a zero-range delta interaction (DI) $V_{\rm pair} = V_\nu^{\rm (DI)}\delta(r_1 - r_2)$ as pairing force, and as alternative recipe we use the density-dependent delta-interaction (DDDI) [22–24] $V_{\rm pair} = V_\nu^{\rm (DDDI)}\delta(r_1 - r_2)\,[1 - \rho(\bar{r})/\rho_0]$. In both cases, ν stands for protons or neutrons. The pairing strengths $V_\nu^{\rm (DI)}$ or $V_\nu^{\rm (DDDI)}$ are adjusted such that the average pairing gaps $\bar{\Delta} = \sum \alpha u_\alpha v_\alpha \Delta_\alpha / \sum \alpha u_\alpha v_\alpha$ [25] are fitted to the pairing gaps from the experimental odd-even staggering of binding energies in a few representative semi-magic nuclei. Actually, we use Sn isotopes for the neutron gaps, namely $\Delta_n(^{112}\mathrm{Sn}) = 1.41\,\mathrm{MeV}$, $\Delta_n(^{120}\mathrm{Sn}) = 1.39\,\mathrm{MeV}$, $\Delta_n(^{124}\mathrm{Sn}) = 1.31\,\mathrm{MeV}$, and some $N = 82$ isotones for the proton gaps $\Delta_n(^{136}\mathrm{Xe}) = 0.98\,\mathrm{MeV}$, $\Delta_n(^{144}\mathrm{Sa}) = 1.25\,\mathrm{MeV}$. The adjustment is done for each force separately because the much different effective masses call for different pairing strengths in each case. The gaps are well fitted in the average (better than 1%). The trends are reproduced within at least 10% precision.

Table 1. Nuclear matter properties for the considered forces: saturation density $\rho_{\rm nm}$ in units of fm^{-3}, binding energy E/A in units of MeV, incompressibility K_∞ in units of MeV, isoscalar effective mass m^*/m, symmetry energy $a_{\rm sym}$ in units of MeV, and sum rule enhancement factor $\kappa_{\rm TRK}$ (equivalent to isovector effective mass).

Force	$\rho_{\rm nm}$	$\frac{E}{A}$	K_∞	$\frac{m^*}{m}$	$a_{\rm sym}$	$\kappa_{\rm TRK}$
SkM*	0.160	−15.8	217	0.79	30	0.53
SLy6	0.159	−15.9	230	0.69	32	0.25
SkI3	0.158	−16.0	258	0.58	34	0.25
SkO4	0.161	−15.8	224	0.90	32	0.17
NL-Z2	0.151	−16.2	173	0.58	42	0.72
NL3	0.148	−16.2	272	0.60	37	0.68
PC-F1	0.151	−16.2	270	0.61	38	0.70

The basic properties of these forces in terms of nuclear matter parameters are given in table 1. A detailed discussion is found in [11]. There are the typical systematical differences between RMF and SHF for the symmetry energy and for the sum rule enhancement $\kappa_{\rm TRK}$. These may be related to different slopes in the spherical shell gaps as seen in forthcoming figures. Note, in particular, the large span of effective masses for SHF which cover the range from 0.58 to 0.9 and which is the most important variation because the effective mass has an influence on the spectral gap as well as on deformation and correlation properties.

2.2 Collective correlations

The Cd and Te isotopes far away from the magic neutron shell $N = 82$ turn out to be extremely soft in quadrupole deformations. Their ground state goes beyond a pure mean-field description. It is, in fact, a coherent superposition of mean-field states at various deformations. This means that we include some correlations, namely those associated with low-energy collective motion. The effective energy functionals can still be used for that task as low-energy collective motion can be derived as the adiabatic limit of time-dependent mean fields [26–28]. As practical procedure, we employ the generator-coordinate method (GCM) with Gaussian overlap approximation (GOA), see *e.g.* [28,29]. In fact, we use a variant of GOA which takes care of the topology of coupled rotations and quadrupole vibrations [30–32]. We summarize here briefly the basic ingredients. Details are found in [33,34].

A series of collectively deformed mean-field states $|\Phi_q\rangle$ is generated by quadrupole-constrained Skyrme-Hartree-Fock where q stands for the actual quadrupole momentum. Their energy expectation value $\mathcal{V}(q) = \langle\Phi_q|\hat{H}|\Phi_q\rangle$ provides a raw collective potential in quadrupole space. The path does also define the collective momentum as generator for deformation $\hat{P}_q|\Phi_q\rangle = \imath\partial_q|\Phi_q\rangle$. Collective masses and moments of inertia are computed by linear response to deformation, *i.e.* $\mathcal{M}_q^{-1} = \langle[\hat{R}_q,[\hat{H},\hat{R}_q]]\rangle$, where $\hat{R}_q$ is

defined from linear response to $\hat{P}_q$, *i.e.* $[\hat{H}, \hat{R}_q] \propto \hat{P}_q$, and similarly to rotation (ATDHF cranking). Zero-point energies $E^{(\mathrm{ZPE})}$ for vibrations and rotations are computed from the fluctuations in quadrupole $\langle \hat{P}_q^2 \rangle$ and angular momentum $\langle \hat{J} \rangle$ together with the associated masses. These constitute quantum corrections to the collective potential [35,36,13]. The true collective potential V is then obtained from the raw potential $\mathcal{V}$ as

$$V = \mathcal{V} - E^{(\mathrm{ZPE})} \quad .$$

All ingredients together finally yield a generalized collective Bohr-Hamiltonian

$$\hat{H}^{(\mathrm{coll})} = -\frac{1}{\beta^4}\partial_\beta B \beta^4 \partial_\beta - \frac{1}{\beta^2 \sin 3\gamma}\,\partial_\gamma B_\gamma \sin 3\gamma\, \partial_\gamma + \sum_{k=1}^{3} \frac{\hat{L}_k'^2}{2\Theta_k} + V\,,$$

where the potential V and masses B, Θ are functions of deformation β, γ. The dependence on triaxiality γ is obtained by interpolation of axial results, a procedure which is justified for the nearly spherical nuclei considered here. The ground-state solution in collective space then represents the collectively correlated ground-state energy. The physical collective zero-point energy is, of course, positive, but the quantum corrections which are subtracted from the raw potential are larger, so that at the end we obtain a more tightly bound correlated ground state.

3 Results and discussion

3.1 The effect of ground-state deformation

The mean-field description of nuclei provides the full details of the single-nucleon energies ϵ_k as eigenvalues of the single-particle Hamiltonian. With this information at hand, shell effects can be easily quantified in various manners, *e.g.* as the spectral gap which is the energy difference between the highest occupied state and the lowest unoccupied state (called HOMO-LUMO gap in molecular physics) or as the shell correction energy [37,38] (for a recent analysis in super-heavy elements, see *e.g.* [11]). There is, however, no direct experimental access to single-nucleon spectra due to rearrangement and core polarization effects [6,7]. There remains as a fairly simple and experimental criterion the two-nucleon shell gaps from which we discuss here in particular the two-proton shell gaps

$$\delta_{2p}(Z,N) = \left(E(Z-2) - 2E(Z) + E(Z+2)\right)\Big|_N\,,$$

where $|_N$ means that all energies are taken at the same neutron number N. The δ_{2p} are just the second differences of binding energies. That observable is close to twice the spectral gap in the nucleus with (N, Z), provided that the mean field does not undergo substantial changes from one nucleus to the next. In an earlier publication, we had investigated the two-proton shell gap in the chain of Pb isotopes and we found that deformation softness can indeed lead to strong changes in the mean field which, in turn, modify the two-nucleon gaps [10]. This helped to clarify a puzzle: the experimental two-proton gaps hint a "shell quenching" towards the proton drip line, while spherical mean-field calculations show always a large and robust spectral gap. The quenching seen for the δ_{2p} is an effect of deformation popping up in the step from $Z=50$ to the neighbors with $Z = 50 \pm 2$. Proper inclusion of ground-state deformation delivered nice agreement between mean-field calculations and data. We are now going to explore such effects for the chain of Sn isotopes.

Figure 1 summarizes results from spherical and deformed mean-field calculations. The upper panels show the spectral gaps in Sn isotopes. Within the SHF forces they show a clear dependence on the effective mass: the gaps increase with decreasing m^*/m. The comparison with RMF hints that the symmetry energy has an impact on the trend with neutron number. However, the gaps from RMF are a bit lower than expected from the very low effective masses in RMF. The reasons for that are still unclear.

The middle panels of fig. 1 show the δ_{2p} from spherical mean-field calculations. At first glance, they behave much similar to the spectral gap (upper panels), as expected. There are, however, changes in quantitative detail due to spherical polarization and rearrangement effects. The values are generally downshifted by 1–2 MeV and the dependence on m^*/m is reduced. Nonetheless, these corrections still stay sufficiently small [7] to leave δ_{2p} as approximate measure of the spectral shell gaps. On the other hand the spherical δ_{2p} are far from the data and the deviation increases with decreasing neutron number.

The lowest panels of fig. 1 show results from axially deformed mean-field calculations. The deformation when active lowers the δ_{2p} because the neighboring isotones gain binding energy through deformation while Sn remains spherical. In order to illustrate the mechanism, we separate the energies into (leading) spherical part and the contribution from deformation:

$$\delta_{2p}(Z,N) = \delta_{2p}^{(0)}(Z,N) + \delta_{2p}^{(\mathrm{d})}(Z,N)\,,$$
$$\delta_{2p}^{(0)}(Z,N) = \left(E^{(0)}(Z-2) - 2E^{(0)}(Z) + E^{(0)}(Z+2)\right)\Big|_N\,,$$
$$\delta_{2p}^{(\mathrm{d})}(Z,N) = \left(E^{(\mathrm{d})}(Z-2) + E^{(\mathrm{d})}(Z+2)\right)\Big|_N < 0\,.$$

$E^{(0)}$ is the energy of the spherical configuration. $E^{(\mathrm{d})}$ is the gain in binding through deformation, thus $E^{(\mathrm{d})} < 0$. The Sn isotopes, the intermediate chain, stay spherical while the softer neighbors Cd and Te develop deformation. This produces the unique direction for the deformation effect on δ_{2p} for Sn. The detailed deformation energies for the considered nuclei are shown in fig. 2. Comparing that with the lowest panels of fig. 1 confirms that the reduction of the δ_{2p} around $N \approx 60$ originates from the deformation of the neighboring nuclei. All forces show the deformation effect towards the side of lower N, but the onset of this effect differs, mainly due to the differences in effective mass [39].

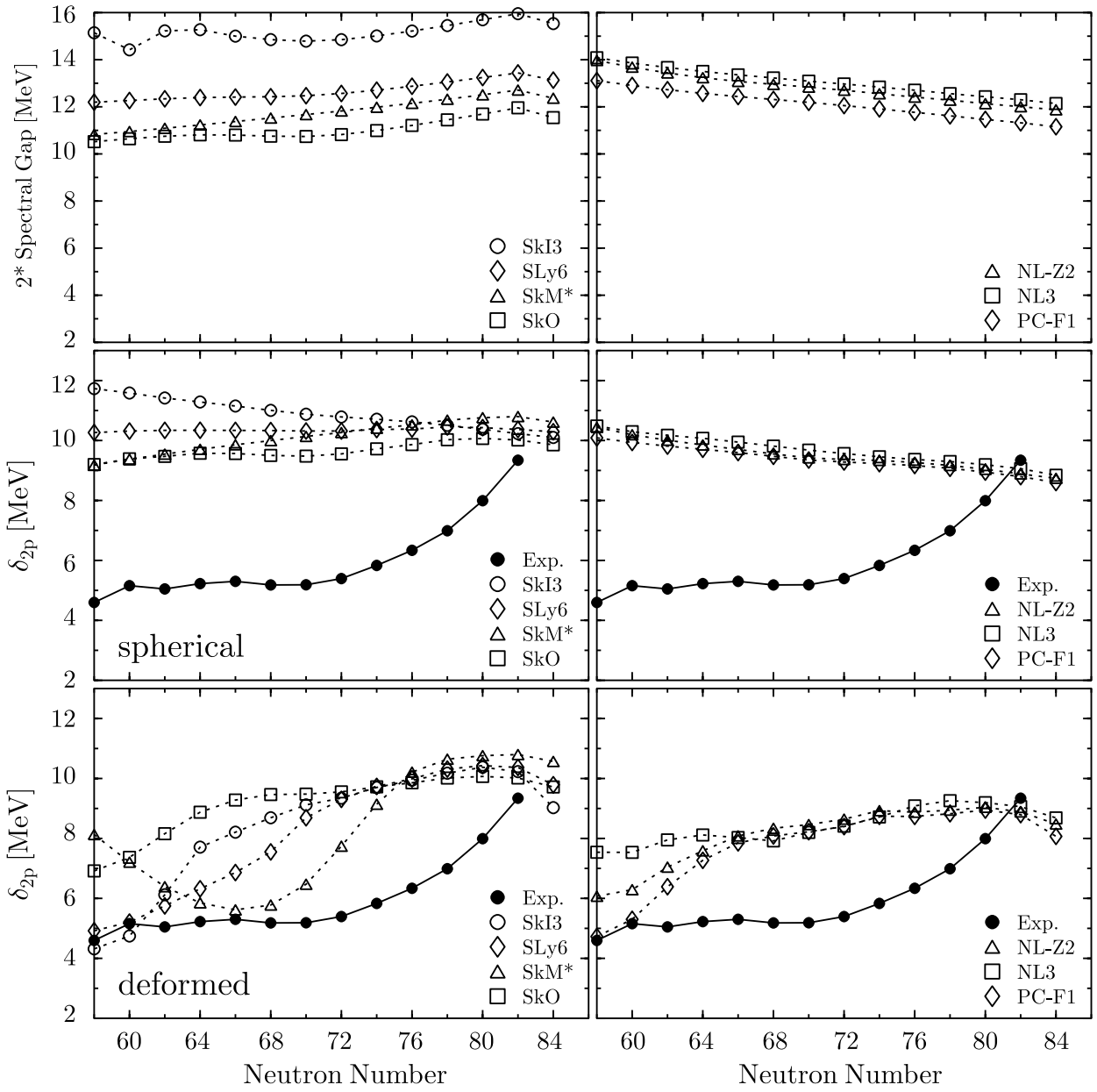

Fig. 1. Upper panels: twice the spectral gap for protons (difference between lowest unoccupied and highest occupied proton state) along the chain of Sn isotopes. Middle panels: two-proton shell gaps δ_{2p} calculated in the spherical mean field. Lower panels: two-proton shell gaps δ_{2p} calculated in the axially deformed mean field. The left panels shows results from various SHF parameterizations as indicated and the right panels from RMF ones.

The lower m^*/m the later (in terms of low N) the onset. The RMF results, for example, deform only for low N and stay closer to each other with respect to the onset of deformations because they have all about the same low m^*/m. The case of SkO is an exception to that rule. Note that this force was fitted with somewhat different conditions, namely a strong constraint on the two-neutron shell gap in ^{208}Pb [19]. This seems to have deep consequences on the shell structure with side-effects as observed here, and in the forthcoming figures. Related to the shifted onsets is a shift of the minima in the curves. The first force showing up with deformations, SkM*, is also the first to return to sphericity when approaching the lower neutron shell closure at $N = 50$. Thus we see a clear maximum of deformation effects within the plotting window. The other forces will bend up as well, but outside the plotting window. In spite of the variations in the results, all models still overestimate the two-proton shell-gap in the region $N = 72$–80 as seen clearly in the lower panels of fig. 1.

3.2 The impact of ground-state correlations

A possible reason for that may be ground-state correlations (GSC). Nuclei near the onset of deformation are

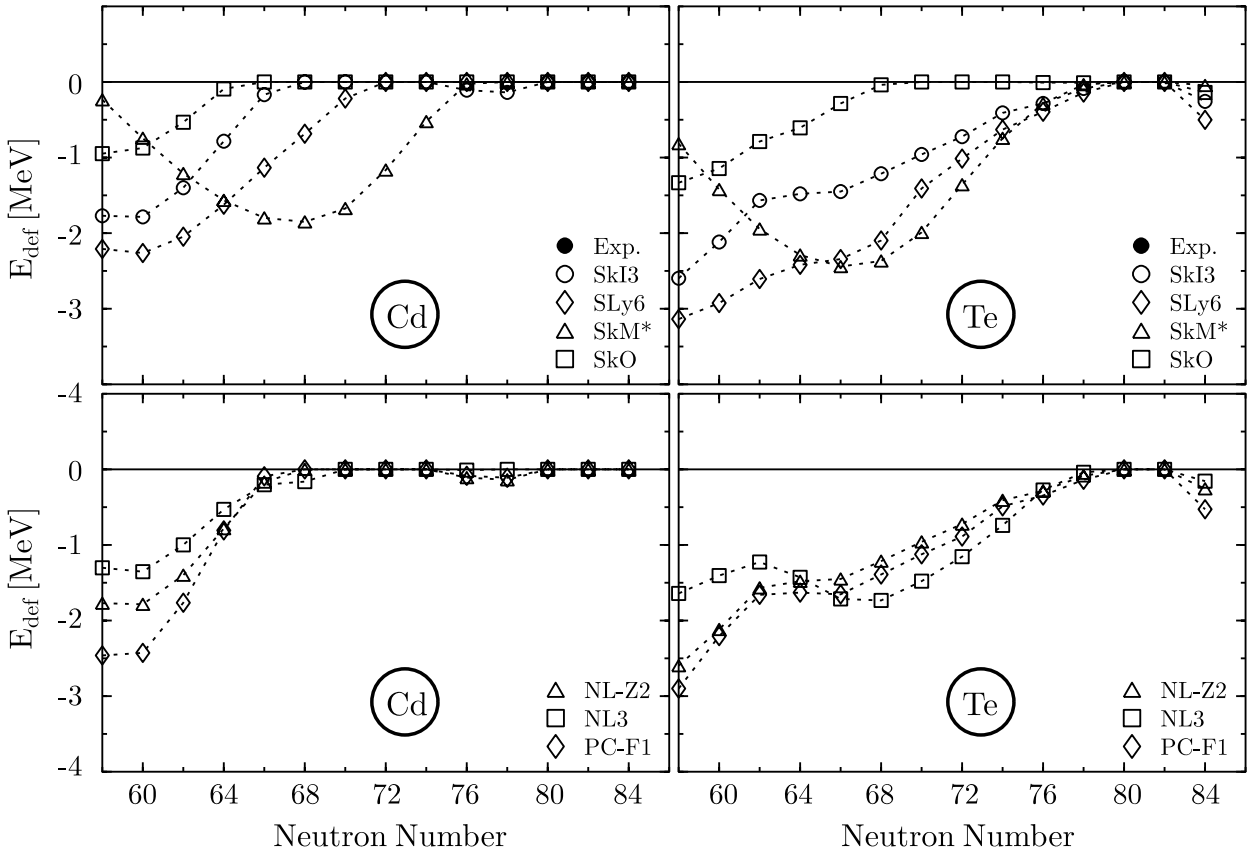

Fig. 2. The deformation energy $E^{(\mathrm{d})}$ in the neighboring isotopic chains Cd and Te for the various forces as indicated.

usually soft against quadrupole fluctuations even if the mean deformation still stays close to sphericity. These quadrupole quantum fluctuations in the ground state lead to a correlation which also produces extra binding. The Sn nuclei are more rigid (owing to the proton shell closure $Z = 50$) than their neighbors and thus we can expect a further lowering of the δ_{2p} particularly in the transitional region. The effect on the δ_{2p} is demonstrated in fig. 3 for the force SkI3 as test case. We again see the significant step towards the experimental trend when switching from spherical to deformed mean-field calculations. The next step is to account for the GSC and this indeed provides the expected additional lowering of the δ_{2p}. The effect is particularly pronounced in the transitional region where the deformation effect alone is still too small. However, it is not yet large enough to reach agreement with the data. As an aside, we note the somewhat strange detail at $N = 82$ where the correlation effect even changes sign. The nucleus ^{132}Sn is doubly magic and we suspect that the simple pairing treatment is a bit risky in the immediate vicinity of a double shell closure, and it is just this vicinity which contributes to the δ_{2p}. On the other hand, the effect remains rather small and well localized. It stays away from the transitional region which is the focus of our discussions.

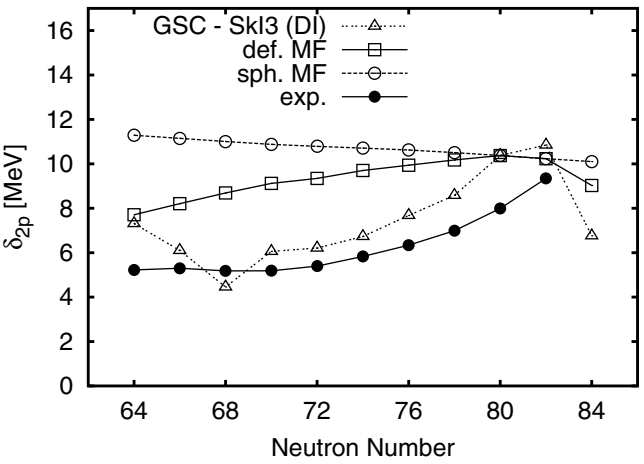

Fig. 3. The two-proton shell gap δ_{2p} calculated for the interaction SkI3 with spherical mean field, deformed mean field, and with collective GSC from quadrupole fluctuations (computed as sketched in sect. 2.2). All cases used DI pairing. The experimental data is taken from [3]

Complementing information on the correlation effect is provided in fig. 4. The upper panel shows the squared quadrupole expectation value $\langle \hat{\beta}_2^2 \rangle$ for the correlated state. It embraces the ground-state deformation as well as the collective fluctuations. The fluctuation part is to a good approximation proportional to the $B(E2)$ values. The total $\langle \hat{\beta}_2^2 \rangle$ is directly related to the correlation effect on the r.m.s. radii [40,41]. There is, however, not such a direct relation to the correlation energy as can be seen from comparison with the lower part of the figure. The reason is

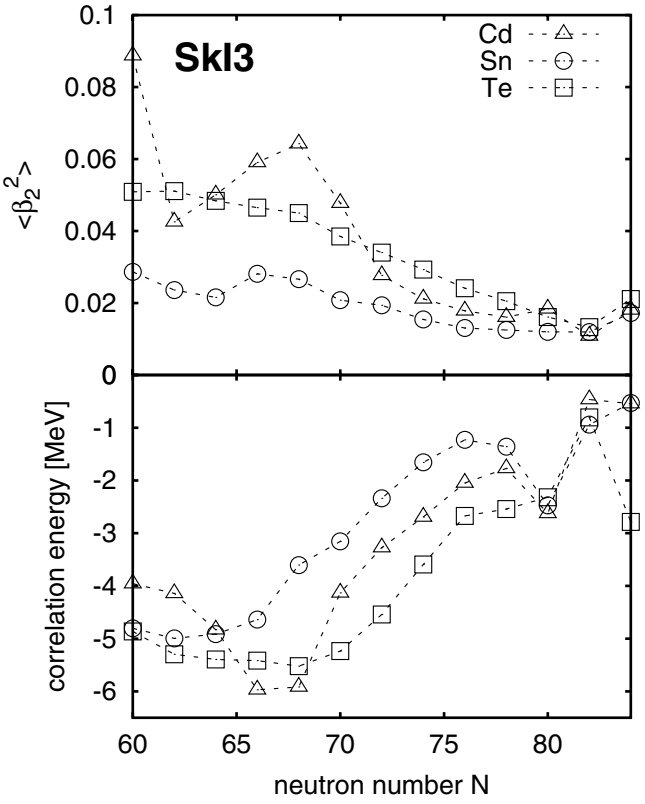

Fig. 4. Details for the correlation effect with SkI3 and DI pairing. Upper panel: the squared quadrupole expectation value $\langle\hat{\beta}_2^2\rangle$ for Sn and its even neighbors. Lower panel: the correlation energy (difference between fully correlated ground-state energy and the deformed mean-field minimum).

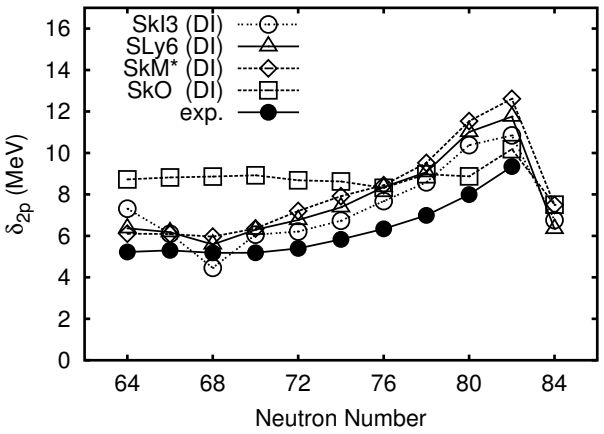

Fig. 5. Computed δ_{2p} including the quadrupole ground-state correlations (GSC) for the three Skyrme interactions SkI3, SLy6 and SkM* all using delta interaction (DI) pairing. The experimental data are taken from [3]

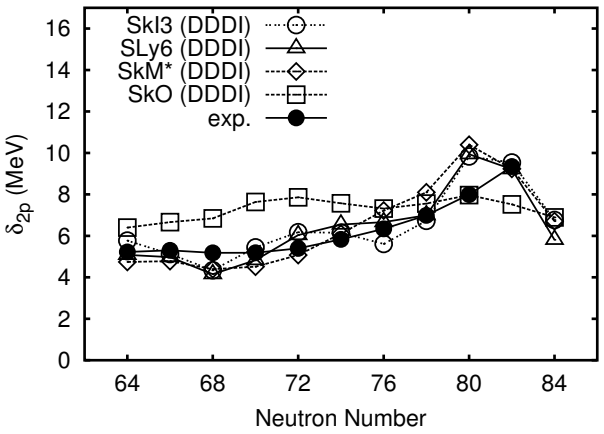

Fig. 6. As fig. 5, but with DDDI pairing.

that the correlation energy is composed of two counteracting contributions, the negative quantum correction energy (see sect. 2.2) and the positive collective zero-point energy. The $\langle\hat{\beta}_2^2\rangle$ is small for the semi-magic Sn isotopes, while it grows systematically towards mid-shell for the neighboring elements Cd and Te. This shows that collective vibrations are much softer for these nuclei. The correlation energy, on the other hand, grows towards mid-shell for all three elements. But it is larger for Cd and Te in the transitional region such that finally the correlations just serve to fill the gap between deformed results (lower panel in fig. 1) and experiment.

In order to exclude that this may be a particular problem of the force SkI3 (used for fig. 3) in fig. 5 results with GSC and for a broader variety of Skyrme forces are shown. The force SkO (having a rather large effective mass $m^*/m = 0.9$) is even farther away from the data, even when including deformation and GSC as done here. The other forces yield on the average the same result as we had seen for SkI3 before. It is interesting to note that the actual size of the correlation effect differs amongst the forces as can be seen from the fact that the ordering of the results in relation to data is different as in the deformed mean field shown in fig. 1. The force SkI3 is a bit special as it shows some fluctuations at neutron number $N = 68$ which appear only when correlations are included. This is due to a small sub-shell closure which exists for SkI3 and not for the other three forces. In spite of the observed variances of the results, none of them reaches fully near the data in a systematic manner.

Thus far we have considered a certain variation of Skyrme forces. Pairing is the other crucial ingredient in the effective energy functional. Up to now, we have considered only the DI pairing. A widely used alternative is the surface, or DDDI, pairing. Figure 6 shows results of calculations with ground-state correlations using the same Skyrme forces as above, but now with DDDI pairing. The force SkO behaves again a bit strange. The alternative pairing recipe helps a bit but cannot counterweight the obviously inappropriate mean-field background of this particular parameterization. The main effect is that DDDI pairing reduces the two-proton shell gap by about one more MeV and this brings the results for the three well-performing forces (SkM*, SLy6, SkI3) on top of the experimental data. The effect of DDDI *versus* DI pairing is only about 1 MeV for that subtle observable δ_{2p}, but crucial for

final success. The difference comes mainly from the neighboring isotones Cd and Te which are a bit less soft with DDDI. The example is one hint that DDDI pairing may be more realistic, but much more evidence has yet to be collected to support such a statement, see *e.g.* the many discussion of that question from different aspects in [42–44].

4 Conclusions

We have investigated the two-proton shell gap in Sn isotopes in the framework of self-consistent mean-field models, the Skyrme-Hartree-Fock approach as well as the relativistic mean-field model. In a first step beyond pure mean field, we have also considered the effect of collective correlations stemming from quadrupole vibrations. In order to work out systematic trends, we have considered a variety of different parameterizations in both mean-field models.

In a first step, we have investigated the effect of ground-state deformations on the two-proton shell gap. In both trend and order of magnitude the results were quite similar to those of a previous study on Pb isotopes thus corroborating that effect as a general feature for all nuclei. The deformation effects are negligible only near the doubly magic nuclei and take over as soon as the neutron number is sufficiently far from a magic shell closure.

Different from our earlier studies on Pb isotopes, the resulting two-proton shell gaps did not match the experimental data even when including the deformation effects. Thus we have also checked the impact of collective ground-state correlations. They do indeed lower the two-proton shell gap in the critical region by about 1–2 MeV and thus bring the results closer to the data. It was then found that a further crucial ingredient is the pairing model. We compared a delta interaction (DI) pairing with a density-dependent delta interaction (DDDI). There is again about 1 MeV difference in the results. The DDDI pairing together with the collective ground-state correlations finally delivers a perfect agreement with the experimental data for a variety of different Skyrme forces.

In summary, the results show that the two-proton shell gap is a very subtle observable which is extremely sensitive to various details of the treatment, spherical and deformed polarization effects as well as correlations. The final result reflects different features of the forces as, *e.g.*, the effective mass (which defines the underlying spectral gap) and the various response parameters (which enter the polarization effects). The two-nucleon shell gaps certainly provide useful information about nuclear shell structure. But the situation is similarly involved as with single-nucleon information from odd nuclei. It requires a careful consideration of all ingredients to compare theory with experimental data.

The authors thank M. Bender for many inspiring discussions and helpful remarks. This work was supported in part by the Bundesministerium für Bildung und Forschung (BMBF), Project Nos. 06 ER 808 and 06 ER 124.

References

1. M. Göppert-Mayer, Phys. Rev. **75**, 1969 (1949).
2. O. Haxel, J.H.D. Jensen, H.E. Suess, Phys. Rev. **75**, 1766 (1949).
3. T. Radon, H. Geissel, G. Münzenberg, B. Franzke, T. Kerscher, F. Nolden, Y.N. Novikov, Z. Patyk, C. Scheidenberger, F. Attallah, K. Beckert, T. Beha, F. Bosch, H. Eickhoff, M. Falch, Y. Fujita, M. Hausmann, F. Herfurth, H. Irnich, H.C. Jung, O. Klepper, C. Kozhuharov, Y.A. Litvinov, K.E.G. Löbner, F. Nickel, H. Reich, W. Schwab, B. Schlitt, M. Steck, K. Sümmerer, T. Winkler, H. Wollnik, Nucl. Phys. A **677**, 75 (2000).
4. P.-G. Reinhard, M. Bender, J.A. Maruhn, Commun. Mod. Phys. A **2**, 177 (2002).
5. M. Bender, W. Nazarewicz, P.-G. Reinhard, Phys. Lett. B **515**, 42 (2001).
6. V. Bernard, Nguyen Van Giai, Nucl. Phys. A **348**, 75 (1980).
7. K. Rutz, M. Bender, P.-G. Reinhard, J.A. Maruhn, W. Greiner, Nucl. Phys. A **634**, 67 (1998).
8. M. Bender, K. Rutz, P.-G. Reinhard, J.A. Maruhn, W. Greiner, Phys. Rev. C **60**, 034304 (1999).
9. Y.N. Novikov, F. Attallah, F. Bosch, M. Falch, H. Geissel, M. Hausmann, T. Kerscher, O. Klepper, H.-J. Kluge, C. Kozhuharov, Y.A. Litvinov, K.E.G. Löbner, G. Münzenberg, Z. Patyk, T. Radon, C. Scheidenberger, A.H. Wapstra, H. Wollnik, Nucl. Phys. A **697**, 92 (2002).
10. M. Bender, T. Cornelius, G. Lalazissis, J. Maruhn, W. Nazarewicz, P.-G. Reinhard, Eur. Phys. J. A **14**, 23 (2002).
11. M. Bender, P.-H. Heenen, P.-G. Reinhard, Rev. Mod. Phys. **75**, 121 (2003).
12. B.D. Serot, J.D. Walecka, Adv. Nucl. Phys. **16**, 1 (1986).
13. P.-G. Reinhard, Rep. Prog. Phys. **52**, 439 (1989).
14. B.A. Nikolaus, T. Hoch, D.G. Madland, Phys. Rev. C **46**, 1757 (1992).
15. T. Bürvenich, D.G. Madland, J.A. Maruhn, P.-G. Reinhard, Phys. Rev. C **65**, 044308 (2002).
16. J. Bartel, P. Quentin, M. Brack, C. Guet, H.-B. Håkansson, Nucl. Phys. A **386**, 79 (1982).
17. E. Chabanat, P. Bonche, P. Haensel, J. Meyer, R. Schaeffer, Nucl. Phys. A **627**, 710 (1997).
18. P.-G. Reinhard, H. Flocard, Nucl. Phys. A **584**, 467 (1995).
19. P.-G. Reinhard, D.J. Dean, W. Nazarewicz, J. Dobaczewski, J.A. Maruhn, M.R. Strayer, Phys. Rev. C **60**, 014316 (1999).
20. M. Bender, Phys. Rev. C **61**, 031302(R) (2000).
21. Y.K. Gambhir, P. Ring, A. Thimet, Ann. Phys. (N.Y.) **198**, 132 (1990).
22. F. Tondeur, Nucl. Phys. A **315**, 353 (1979).
23. S.J. Krieger, P. Bonche, H. Flocard, P. Quentin, M.S. Weiss, Nucl. Phys. A **517**, 275 (1990).
24. J. Terasaki, P.-H. Heenen, P. Bonche, J. Dobaczewski, H. Flocard, Nucl. Phys. A **593**, 1 (1995).
25. M. Bender, K. Rutz, P.-G. Reinhard, J. Maruhn, Eur. Phys. J. A **8**, 59 (2000).
26. M. Baranger, M. Véneroni, Ann. Phys. (N.Y.) **114**, 123 (1978).
27. K. Goeke, P.-G. Reinhard, Ann. Phys. (N.Y.) **112**, 328 (1978).
28. P.-G. Reinhard, K. Goeke, Rep. Prog. Phys. **50**, 1 (1987).

29. P. Bonche, J. Dobaczewski, H. Flocard, P.-H. Heenen, J. Meyer, Nucl. Phys. A **510**, 466 (1990).
30. P.-G. Reinhard, Z. Phys. A **285**, 93 (1978).
31. K. Hagino, P.-G. Reinhard, G. Bertsch, Phys. Rev. C **65**, 064320 (2002).
32. K. Hagino, G. Bertsch, P.-G. Reinhard, Phys. Rev. C **68**, 024306 (2003).
33. P. Fleischer, PhD Thesis, Universität, Erlangen/Germany, 2003.
34. P. Fleischer, P. Klüpfel, P.-G. Reinhard, J.A. Maruhn, to be published in Phys. Rev. C.
35. P.-G. Reinhard, Nucl. Phys. A **252**, 120 (1975).
36. P.-G. Reinhard, Nucl. Phys. A **261**, 291 (1976).
37. V. Strutinski, Nucl. Phys. A **95**, 420 (1967).
38. M. Brack, J. Damgård, A. Jensen, H. Pauli, V. Strutinski, C. Wong, Rev. Mod. Phys. **44**, 320 (1972).
39. V. Blum, J. Fink, P.-G. Reinhard, J.A. Maruhn, W. Greiner, Phys. Lett. B **223**, 123 (1989).
40. P.-G. Reinhard, D. Drechsel, Z. Phys. A **290**, 85 (1979).
41. F. Barranco, R.A. Broglia, Phys. Lett. B **151**, 90 (1985).
42. A. Avdeenkov, S. Kamerdzhiev, JETP Lett. **69**, 715 (1999).
43. J. Dobaczewski, W. Nazarewicz, M. Stoitsov, Eur. Phys. J. A **15**, 21 (2002).
44. T. Duguet, Phys. Rev. C **69**, 054317 (2004).